The Astronomical Journal, 129:2519–2530, 2005 June
© 2005. The American Astronomical Society. All rights reserved. Printed in U.S.A.

X-RAY LIGHTHOUSES OF THE HIGH-REDSHIFT UNIVERSE. II. FURTHER SNAPSHOT OBSERVATIONS OF THE MOST LUMINOUS $z \gtrsim 4$ QUASARS WITH *CHANDRA*

C. Vignali,[1,2] W. N. Brandt,[3] D. P. Schneider,[3] and S. Kaspi[4,5]

Received 2004 October 18; accepted 2005 March 13

ABSTRACT

We report on *Chandra* observations of a sample of 11 optically luminous ($M_B < -28.5$) quasars at $z = 3.96$–4.55 selected from the Palomar Digital Sky Survey and the Automatic Plate Measuring Facility Survey. These are among the most luminous $z \gtrsim 4$ quasars known and hence represent ideal witnesses of the end of the "dark age." Nine quasars are detected by *Chandra*, with ≈2–57 counts in the observed 0.5–8 keV band. These detections increase the number of X-ray-detected AGNs at $z \gtrsim 4$ to ≈90; overall, *Chandra* has detected ≈85% of the high-redshift quasars observed with snapshot (few kilosecond) observations. PSS 1506+5220, one of the two X-ray-undetected quasars, displays a number of notable features in its rest-frame ultraviolet spectrum, the most prominent being broad, deep Si IV and C IV absorption lines. The average optical-to-X-ray spectral index for the present sample ($\langle \alpha_{ox} \rangle = -1.88 \pm 0.05$) is steeper than that typically found for $z \gtrsim 4$ quasars but consistent with the expected value from the known dependence of this spectral index on quasar luminosity.

We present joint X-ray spectral fitting for a sample of 48 radio-quiet quasars in the redshift range 3.99–6.28 for which *Chandra* observations are available. The X-ray spectrum (≈870 counts) is well parameterized by a power law with $\Gamma = 1.93^{+0.10}_{-0.09}$ in the rest-frame ≈2–40 keV band, and a tight upper limit of $N_H \approx 5 \times 10^{21}$ cm^{-2} is obtained on any average intrinsic X-ray absorption. There is no indication of any significant evolution in the X-ray properties of quasars between redshifts 0 and 6, suggesting that the physical processes of accretion onto massive black holes have not changed over the bulk of cosmic time.

Key words: galaxies: active — galaxies: nuclei — quasars: general — X-rays: galaxies

1. INTRODUCTION

Over the last few years, X-ray observations have provided important information about the population of luminous quasars populating the universe at $z \approx 4$–6, i.e., at the end of the "dark age" (e.g., Rees 1999). Since the work by Kaspi et al. (2000) with archival *ROSAT* observations, X-ray studies of high-redshift quasars have taken advantage of the capabilities of the new generation of X-ray observatories: *Chandra* and *XMM-Newton*. In particular, *Chandra* snapshot observations of $z \gtrsim 4$ active galactic nuclei (AGNs) have proven to be effective in providing basic X-ray information, such as X-ray fluxes, luminosities, and broadband properties, on some of the most luminous objects in the universe (Vignali et al. 2001a, 2002, 2003b, 2003c, hereafter V01a, V02, V03b, and V03c, respectively; Brandt et al. 2002; Bechtold et al. 2003; Bassett et al. 2004). Using these observations, it has also been possible to collect enough source counts to allow joint X-ray spectral fitting (V03b; V03c; Vignali et al. 2004). This kind of X-ray study is enabled by the sharp on-axis point-spread function and the low instrumental background of *Chandra*. On the other hand, *XMM-Newton*, with its larger effective area, has allowed individual X-ray spectral fitting for a handful of the most X-ray-luminous $z > 4$ quasars with medium-to-long exposures (Ferrero & Brinkmann 2003; Grupe et al. 2004; Farrah et al. 2004; see also the *Chandra* spectral results of the $z = 5.99$ SDSS 130608.26+035626.3 quasar reported recently by Schwartz & Virani 2004).

It has therefore become possible to provide an overall picture of the radio-quiet and radio-loud quasar populations at the highest redshifts. However, X-ray studies of the most optically luminous quasars at $z > 4$ have been conducted for a limited number of objects, the majority of which have been selected from the Digital Palomar Sky Survey (PSS; e.g., Djorgovski et al. 1998) and presented by V03b. The goal of the present study is to extend previous X-ray investigations of the properties of luminous quasars at $z \gtrsim 4$ using *Chandra* snapshot observations; the target sample comprises 11 quasars in the redshift range $z = 3.96$–4.55 ($M_B \approx -28.5$ to -29.5) selected from the PSS and the Automatic Plate Measuring (APM) Facility Survey (BRI; e.g., Irwin et al. 1991; Storrie-Lombardi et al. 1996, 2001). Throughout the paper we adopt $H_0 = 70$ km s^{-1} Mpc^{-1}, $\Omega_M = 0.3$, and $\Omega_\Lambda = 0.7$ (e.g., Spergel et al. 2003).

2. *CHANDRA* OBSERVATIONS AND DATA REDUCTION

All of the quasars presented here were targeted by *Chandra* during Cycle 4 with snapshot (≈4.0–5.1 ks) observations. The observation log is shown in Table 1. All of the sources were observed with the Advanced CCD Imaging Spectrometer (ACIS; Garmire et al. 2003) with the S3 CCD at the aimpoint. Faint mode was used for the event telemetry format, and *ASCA* grade 0, 2, 3, 4, and 6 events were used in the analysis, which was carried out using the *Chandra* Interactive Analysis of Observations (CIAO) version 2.3 software. No background flares are present in these observations. Source detection was carried out with WAVDETECT (Freeman et al. 2002), similarly to V01a, V03b, and V03c, using wavelet transforms (with wavelet scale

[1] Dipartimento di Astronomia, Università degli Studi di Bologna, Via Ranzani 1, 40127 Bologna, Italy; cristian.vignali@bo.astro.it.
[2] INAF–Osservatorio Astronomico di Bologna, Via Ranzani 1, 40127 Bologna, Italy.
[3] Department of Astronomy and Astrophysics, Pennsylvania State University, 525 Davey Laboratory, University Park, PA 16802; niel@astro.psu.edu, dps@astro.psu.edu.
[4] School of Physics and Astronomy, Raymond and Beverly Sackler Faculty of Exact Sciences, Tel Aviv University, Tel Aviv 69978, Israel; shai@wise.tau.ac.il.
[5] Physics Department, Technion, Haifa 32000, Israel.

TABLE 1

Chandra Observations of High-Redshift Quasars

Object Name	z	Optical (α_{2000})	Optical (δ_{2000})	$\Delta_{\mathrm{Opt-X}}$[a] (arcsec)	X-Ray Obs. Date	Exposure Time[b] (ks)	Reference
BR 0331−1622	4.36	03 34 13.4	−16 12 04.8	0.4	2003 Jun 17	4.67	1, 2
BR 0353−3820	4.55	03 55 04.9	−38 11 42.3	0.3	2003 Sep 10	4.06	1, 2
BR 0418−5723	4.46	04 19 50.9	−57 16 13.1	0.7	2003 Jun 15	3.99	1, 2
BR 0424−2209	4.32	04 26 10.3	−22 02 17.6	0.4	2002 Dec 14	4.67	1, 2
PSS 0747+4434	4.43	07 47 49.7	+44 34 16.9	0.5	2002 Dec 17	4.54	1
PSS 1058+1245	4.33	10 58 58.4	+12 45 54.8	0.1	2003 Mar 2–3	5.05	3
BR 1117−1329	3.96	11 20 10.3	−13 46 25.7	0.4	2003 Jan 28	4.70	4
PSS 1506+5220	4.18	15 06 54.5	+52 20 05.2	...	2003 Mar 14	4.86	3
PSS 1646+5514	4.04	16 46 56.4	+55 14 46.4	0.3	2003 Sep 10	4.85	1
BR 2213−6729	4.47	22 16 51.9	−67 14 43.4	0.4	2003 Mar 10	4.90	1, 2
PSS 2344+0342	4.24	23 44 03.2	+03 42 25.5	...	2003 Nov 20	5.10	1

Note.—The optical positions of the quasars have been obtained using SExtractor (Bertin & Arnouts 1996) on the DPOSS2 images, while the X-ray positions have been obtained with WAVDETECT. Units of right ascension are hours, minutes, and seconds, and units of declination are degrees, arcminutes, and arcseconds.

[a] Distance between the optical and X-ray positions; the ellipses indicate no X-ray detection.

[b] The *Chandra* exposure time has been corrected for detector dead time.

References.—(1) Peroux et al. 2001; (2) Storrie-Lombardi et al. 2001; (3) Omont et al. 2001; (4) Storrie-Lombardi et al. 1996.

sizes of 1, 1.4, 2, 2.8, and 4 pixels) and a false positive probability threshold of 10^{-4}. Given the small number of pixels being searched because of the known source positions and the subarcsecond on-axis angular resolution of *Chandra*, the probability of spurious detections is extremely low; most of the sources were in fact detected at a false positive probability threshold of 10^{-6}.

The X-ray counts detected in the ultrasoft band (0.3–0.5 keV), the soft band (0.5–2 keV), the hard band (2–8 keV), and the full band (0.5–8 keV) are reported in Table 2. The counts have been derived using WAVDETECT and checked with manual aperture photometry. Nine quasars have been detected, with full-band counts ranging between 2 and 57. The X-ray positions of the detected sources are within 0.″1–0.″7 of the optical positions; this is consistent with the expected *Chandra* ACIS positional error.

In Table 2 the band ratios and the effective photon indices for the X-ray-detected sources are also reported. Both of these quantities have been corrected for the quantum efficiency decay of ACIS at low energies, caused by molecular contamination of the ACIS filters, using a time-dependent correction. To apply the correction, we adopted the ACISABS model (see, e.g., Chartas et al. 2002).[6] We note that, given the dates of our observations, the differences between the adoption of either this model or that proposed by the *Chandra* X-ray Center (CXC),[7] available with the latest CIAO release, are small; therefore, for consistency with our previous work (e.g., V03b; V03c), we adopt the ACISABS model throughout this paper.

[6] See http://www.astro.psu.edu/users/chartas/xcontdir/xcont.html.

[7] For further details, see http://asc.harvard.edu/ciao/why/acisqedeg.html.

TABLE 2

X-Ray Counts, Band Ratios, and Effective Photon Indices

Object	X-Ray Counts[a] (0.3–0.5 keV)	(0.5–2 keV)	(2–8 keV)	(0.5–8 keV)	Band Ratio[b]	Γ[b]
BR 0331−1622	<3.0	$8.9^{+4.1}_{-2.9}$	$3.9^{+3.2}_{-1.9}$	$12.6^{+4.7}_{-3.5}$	$0.34^{+0.31}_{-0.19}$	$1.6^{+0.7}_{-0.6}$
BR 0353−3820	$4.0^{+3.2}_{-1.9}$	$45.9^{+7.8}_{-6.8}$	$10.9^{+4.4}_{-3.3}$	$56.7^{+8.6}_{-7.5}$	$0.18^{+0.08}_{-0.06}$	2.0 ± 0.3
BR 0418−5723	<3.0	$7.0^{+3.8}_{-2.6}$	<6.4	$9.0^{+4.1}_{-2.9}$	<0.70	>0.8
BR 0424−2209	<4.8	$10.0^{+4.3}_{-3.1}$	<6.4	$11.9^{+4.6}_{-3.4}$	<0.49	>1.2
PSS 0747+4434	<4.8	$6.0^{+3.6}_{-2.4}$	<3.0	$6.0^{+3.6}_{-2.4}$	<0.39	>1.6
PSS 1058+1245	<4.8	$3.0^{+2.9}_{-1.6}$	<6.4	$5.0^{+3.4}_{-2.2}$	<1.64	>0.1
BR 1117−1329	<3.0	$2.0^{+2.7}_{-1.3}$	<3.0	$2.0^{+2.7}_{-1.3}$	<1.15	>0.5
PSS 1506+5220	<3.0	<4.8	<4.8	<6.4	...	...
PSS 1646+5514	<3.0	$6.0^{+3.6}_{-2.4}$	<3.0	$6.0^{+3.6}_{-2.4}$	<0.38	>1.4
BR 2213−6729	<3.0	$17.9^{+5.3}_{-4.2}$	$3.0^{+2.9}_{-1.6}$	$20.9^{+5.7}_{-4.5}$	$0.13^{+0.13}_{-0.07}$	$2.3^{+0.7}_{-0.6}$
PSS 2344+0342	<3.0	<3.0	<3.0	<3.0	...	...

[a] Errors on the X-ray counts were computed according to Tables 1 and 2 of Gehrels (1986) and correspond to the 1 σ level; these were calculated using Poisson statistics. The upper limits are at the 95% confidence level and were computed according to Kraft et al. (1991). For the sake of clarity, upper limits of 3.0, 4.8, and 6.4 indicate that 0, 1, and 2 X-ray counts, respectively, have been found within an extraction region of radius 2″ centered on the optical position of the quasar (considering the background within this source extraction region negligible).

[b] We calculated errors at the ≈ 1 σ level for the band ratio and effective photon index following the "numerical method" described in § 1.7.3 of Lyons (1991); this avoids the failure of the standard approximate variance formula when the number of counts is small (see § 2.4.5 of Eadie et al. 1971). The band ratios and photon indices have been obtained by applying the correction required to account for the ACIS quantum efficiency decay at low energy.

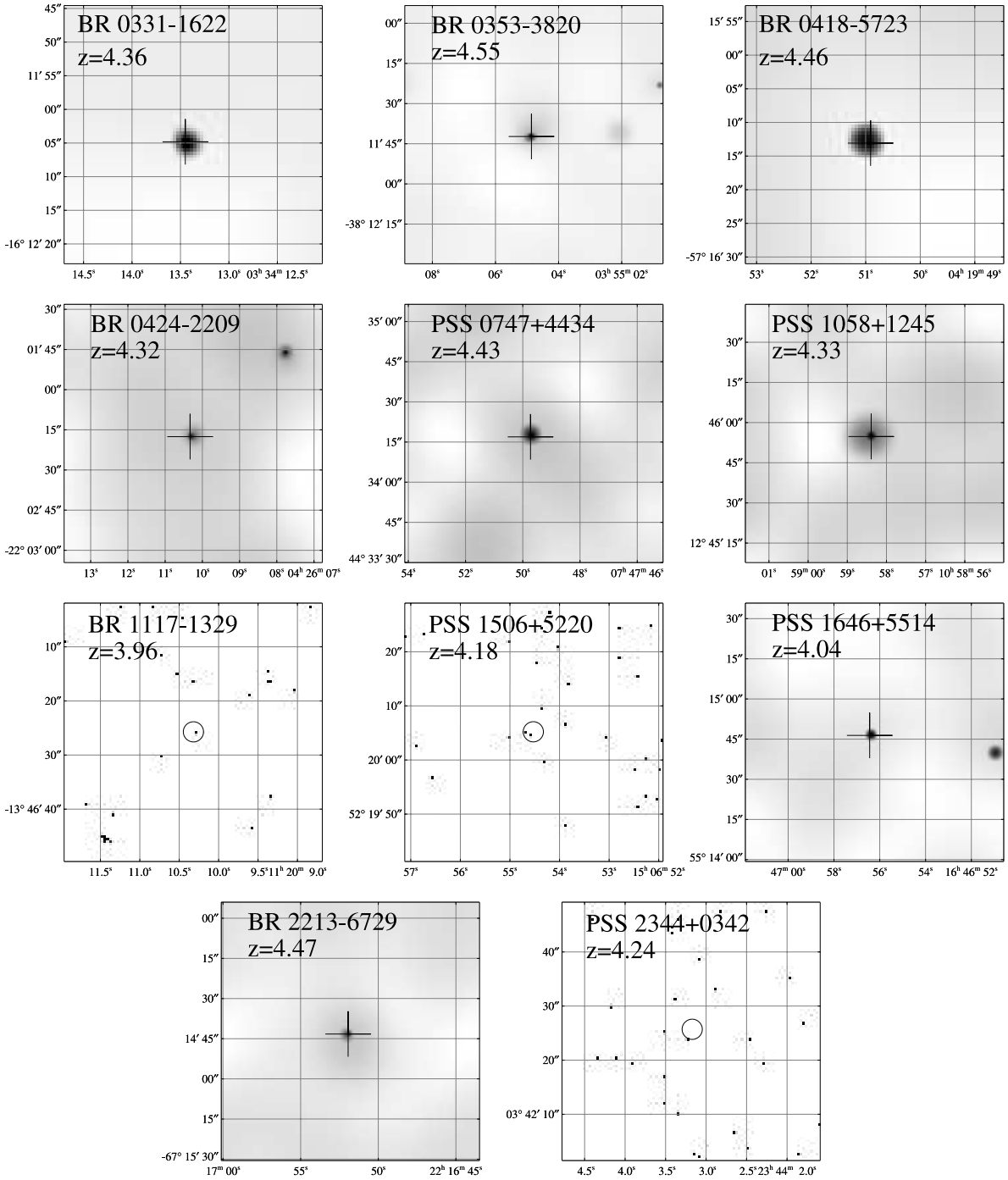

FIG. 1.—Full-band (0.5–8 keV) images of the quasars observed by *Chandra* and presented in this paper. The panels are $98'' \times 98''$ for all of the images, except for the source detected with 2 counts (BR 1117−1329; the 2 counts fall in the same pixel) and those without X-ray detections (PSS 1506+5220 and PSS 2344+0342); for these three sources, the panels are $49'' \times 49''$. North is up, and east is to the left. The images of the sources with >2 counts have been adaptively smoothed at the 2 σ level; the optical positions of the quasars are marked by crosses. For the three sources with $\leq$2 counts, the raw (unsmoothed) images are shown; in these cases, $2''$ radius circles around the optical positions of the quasars are shown. We note that, although two photons fall within the $2''$ radius circle centered on the position of PSS 1506+5220, this is not considered a detection (see § 2.1).

The full-band images of eight detected quasars, adaptively smoothed using the algorithm of Ebeling et al. (2005), are shown in Figure 1. For BR 1117−1329, a known broad absorption-line quasar (BALQSO; Storrie-Lombardi et al. 1996) from which 2 counts have been detected (see § 2.1 for discussion), and the two nondetections, the raw images are shown. Overall, in the regions of projected distance $\approx 650 \times 650$ kpc^2 centered on the quasar positions, we did not find any significant excess of companions with respect to the cumulative number counts from X-ray surveys (e.g., Bauer et al. 2004); this is in agreement with previous X-ray searches around high-redshift quasars (e.g., V03b; V03c). Similarly, the absence of X-ray extension for all of our target quasars suggests that significant gravitational lensing (e.g., Comerford et al. 2002) is not present.

Although the observations are short, we have searched for X-ray variability by analyzing the photon arrival times in the full band using the Kolmogorov-Smirnov test. No significant variability was detected from any of our quasars. This is not

surprising given the small numbers of detected counts and the ≈15 minute rest-frame exposure times.

2.1. *Two-Count Sources: BR 1117−1329 and PSS 1506+5220*

As was the case for the $z = 5.27$ quasar SDSS 1208+0010 (V01a) and the $z = 4.80$ quasar SDSS 0756+4502 (V03c), BR 1117−1329 can also be considered a secure detection with only 2 counts (in the same pixel) in the 0.5–2 keV band. In fact, the source is detected by WAVDETECT using a false positive threshold of 10^{-4}. Monte Carlo simulations (see § 2.1.1 of V03c for details) indicate that the significance of this detection is $\approx 4\,\sigma$ in the soft band. In contrast, PSS 1506+5220 cannot be considered detected (according to a Monte Carlo analysis), although 2 full-band counts are present within the 2″ radius circle centered on its optical position (see Fig. 1).

3. HOBBY-EBERLY TELESCOPE OBSERVATIONS

We conducted imaging and spectroscopic observations of several of the quasars using the 9 m Hobby-Eberly Telescope (HET; Ramsey et al. 1998). These data were taken within 1–10 months of the X-ray observations (≤8 weeks in the quasar rest frames) to minimize the effects of variability in the X-ray/optical comparisons. Variability can introduce significant uncertainties into estimates of key parameters (e.g., the optical-to-X-ray spectral index; see § 4). The observations were all obtained with the Marcario Low-Resolution Spectrograph (LRS; Hill et al. 1998a, 1998b; Cobos Duenas et al. 1998).

3.1. *Photometric Observations*

Two minute *R*-band LRS images were acquired for four of the 11 sources (PSS 0747+4434, 1506+5220, 1646+5514, and 2344+0342) during fall 2003–winter 2004. Using the $\approx 4' \times 4'$ LRS images and finding charts of the fields, it was possible to obtain approximate photometric calibrations using the stellar objects in the fields. Although the level of uncertainty in these comparisons is substantial, we did not detect any significant long-term variations (i.e., more than 50%) in the quasar brightnesses from their published values. To have a uniform analysis, we have adopted the APM magnitudes[8] to derive the optical and broad-band parameters of the quasars.

3.2. *Optical Spectrum of PSS 1506+5220*

Two of the quasars, PSS 1058+1245 and PSS 1506+5220, do not have published spectra. Immediately after acquiring the *R*-band image of PSS 1506+5220 on 2004 January 19 (described in § 3.1), we obtained a 15 minute spectrum of the object using the LRS. The spectrum, which is displayed in Figure 2, was acquired using a 2″ slit, an OG515 blocking filter, and a 600 line mm^{-1} grism; this configuration produced a spectrum covering the wavelength range 6300–9100 Å at a resolving power of ≈1100.

The spectrum displays a number of notable and complex features, the most prominent being broad, deep Si IV and C IV absorption lines between redshifts of about 3.68 and 3.84 (a velocity width of approximately 10,000 km s^{-1}). The sharp rise at the blue end of the spectrum is the red wing of the Lyα emission line. Also present is a strong Mg II absorption doublet (total rest equivalent width [EW] of nearly 7 Å).

The previously reported redshift of PSS 1506+5220 is 4.18;[9] however, accurate redshifts of $z > 4$ BALQSOs are difficult to determine. In Figure 2 we have indicated the expected position of the C IV emission line; no feature is found at this location. There is a suggestion of a broad emission feature centered at 7870 Å; if this is the C IV line, the redshift would be approximately 4.08; there is also a hint of a narrow absorption feature in the midst of this putative emission line.

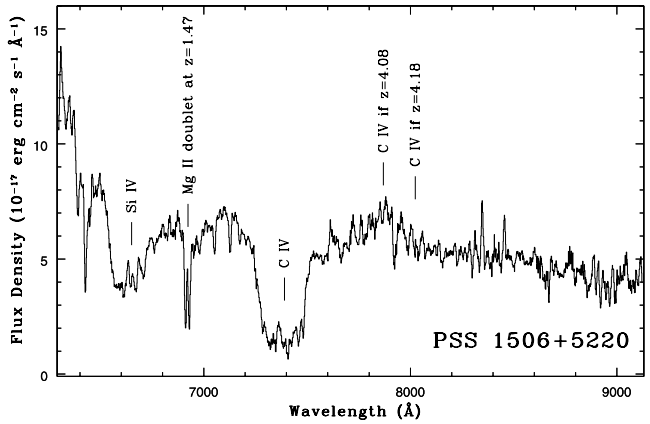

FIG. 2.—Spectrum of PSS 1506+5220 obtained with the LRS of the HET. The data have a spectral resolution of ≈1100. The two prominent broad absorption troughs by Si IV and C IV are labeled, as are the strong Mg II absorption doublet at $z = 1.4711$ and the expected location of the C IV emission line at two redshifts (see § 3.2 for details).

G. Djorgovski has kindly showed an unpublished Keck spectrum of this object to us; his data extend far below the Lyα emission line. If the peak of this line is associated with the rest wavelength of Lyα, then the redshift is indeed 4.18. Given the significant distortions in the lines produced by the absorption troughs, we conclude that it is presently impossible to assign a redshift with an accuracy of better than ≈0.1 for this object. The ejection velocities of the BAL features would range between 20,000 and 25,000 km s^{-1}, depending on the quasar redshift. Throughout the analysis in this paper, we adopt the published value of 4.18 for the redshift of this object.

The strong Mg II absorption feature suggests the presence of a massive galaxy at a redshift of 1.4711 along the line of sight to the quasar. Given this result, the high luminosity of PSS 1506 + 5220 may partially arise from amplification via gravitational lensing.

4. MULTIWAVELENGTH PROPERTIES OF THE SAMPLE

The principal optical, X-ray, and radio properties of our target quasars are listed in Table 3:

Column (1).—The name of the source.

Column (2).—The Galactic column density (from Dickey & Lockman 1990) in units of 10^{20} cm^{-2}.

Column (3).—The monochromatic rest-frame $AB_{1450(1+z)}$ magnitude ($AB_{1450(1+z)} = -2.5 \log f_{1450\ \text{Å}} - 48.6$; Oke & Gunn 1983). The magnitudes reported in Table 3 have been derived from the APM *R*-band magnitudes (corrected for Galactic extinction; Schlegel et al. 1998), assuming the empirical relationship $AB_{1450(1+z)} = R - 0.684z + 3.10$, which is effective in the redshift range covered by our sample.

Columns (4) and (5).—The 2500 Å rest-frame flux density and luminosity. These were computed from the $AB_{1450(1+z)}$ magnitude, assuming an optical power-law slope of $\alpha = -0.79$ ($S_\nu \propto \nu^\alpha$; Fan et al. 2001) to allow direct comparison with the results presented in V01a, V03b, and V03c. Note that the 2500 Å rest-frame flux densities and luminosities are reduced by ≈15% when the power-law slope of the optical continuum is

[8] See http://www.ast.cam.ac.uk/~mike/apmcat/interface.html.
[9] See http://www.astro.caltech.edu/~george/z4.qsos.

TABLE 3

OPTICAL, X-RAY, AND RADIO PROPERTIES OF THE SAMPLE OF HIGH-REDSHIFT QUASARS

Object (1)	N_H[a] (2)	$AB_{1450(1+z)}$ (3)	f_{2500}[b] (4)	$\log(\nu L_\nu)_{2500}$ (5)	M_B (6)	Count Rate[c] (7)	f_X[d] (8)	$f_{2\ keV}$[e] (9)	$\log(\nu L_\nu)_{2\ keV}$ (10)	$\log(L_{2-10\ keV})$[f] (11)	α_{ox}[g] (12)	R[h] (13)
BR 0331−1622.....	5.99	17.7	4.64	47.3	−29.3	$1.90^{+0.88}_{-0.62}$	$8.5^{+4.0}_{-2.8}$	6.81	45.1	45.3	$-1.86^{+0.09}_{-0.08}$	<2.9[i]
BR 0353−3820.....	1.51	17.9	3.86	47.2	−29.2	$11.30^{+1.92}_{-1.68}$	$44.7^{+7.6}_{-6.7}$	37.04	45.8	46.0	$-1.54^{+0.07}_{-0.06}$	5.2[i]
BR 0418−5723.....	1.72	17.8	4.24	47.3	−29.2	$1.76^{+0.95}_{-0.66}$	$7.0^{+3.1}_{-2.6}$	5.69	45.0	45.2	$-1.87^{+0.09}_{-0.10}$	...
BR 0424−2209.....	2.51	18.0	3.52	47.2	−29.0	$2.14^{+0.92}_{-0.66}$	$8.6^{+3.7}_{-2.6}$	6.84	45.1	45.3	-1.81 ± 0.08	<3.8[i]
PSS 0747+4434	5.25	18.4	2.44	47.0	−28.6	$1.32^{+0.79}_{-0.53}$	$5.7^{+3.5}_{-2.2}$	4.66	44.9	45.1	-1.81 ± 0.10	<1.5[j]
PSS 1058+1245	2.05	17.7	4.64	47.3	−29.3	$0.59^{+0.58}_{-0.31}$	$2.4^{+2.3}_{-1.3}$	1.88	44.5	44.7	$-2.07^{+0.13}_{-0.14}$	<0.8[j]
BR 1117−1329.....	5.05	18.3	2.67	47.0	−28.5	$0.43^{+0.57}_{-0.28}$	$1.8^{+2.5}_{-1.2}$	1.37	44.3	44.5	$-2.03^{+0.15}_{-0.18}$	<4.7[i]
PSS 1506+5220	1.68	18.3	2.67	47.0	−28.6	<0.99	<3.9	<3.02	<44.7	<44.9	<−1.90	<1.4[j]
PSS 1646+5514	2.34	17.4	6.12	47.4	−29.5	$1.24^{+0.74}_{-0.50}$	$5.0^{+3.0}_{-2.0}$	3.78	44.8	45.0	-2.00 ± 0.10	<0.1[k]
BR 2213−6729.....	2.73	18.5	2.22	47.0	−28.6	$3.66^{+1.08}_{-0.86}$	$14.9^{+4.4}_{-3.5}$	12.17	45.3	45.5	-1.64 ± 0.07	...
PSS 2344+0342	5.56	18.2	2.93	47.1	−28.8	<0.59	<2.6	<2.05	<44.5	<44.7	<−1.98	<4.5[i]

NOTE.—Luminosities are computed using $H_0 = 70$ km s^{-1} Mpc^{-1}, $\Omega_M = 0.3$, and $\Omega_\Lambda = 0.7$.

[a] From Dickey & Lockman (1990) in units of 10^{20} cm^{-2}.

[b] Rest-frame 2500 Å flux density in units of 10^{-27} ergs cm^{-2} s^{-1} Hz^{-1}.

[c] Observed count rate computed in the 0.5–2 keV band in units of 10^{-3} counts s^{-1}.

[d] Galactic absorption–corrected flux in the observed 0.5–2 keV band in units of 10^{-15} ergs cm^{-2} s^{-1}. These fluxes and the following X-ray parameters have been corrected for the ACIS quantum efficiency decay at low energy.

[e] Rest-frame 2 keV flux density in units of 10^{-32} ergs cm^{-2} s^{-1} Hz^{-1}.

[f] Rest-frame 2–10 keV luminosity in units of ergs per second.

[g] Errors have been computed following the "numerical method" described in § 1.7.3 of Lyons (1991); both the statistical uncertainties on the X-ray count rates and the effects of the observed ranges of the X-ray and optical continuum shapes have been taken into account (see § 3 of V01a for details).

[h] Radio-loudness parameter, defined as $R = f_{5\ GHz}/f_{4400\ Å}$ (rest frame; e.g., Kellermann et al. 1989). The rest-frame 5 GHz flux density is computed from the observed 1.4 GHz flux density (mainly taken from the FIRST and the NVSS) assuming a radio power-law slope of $\alpha = -0.8$, with $f_\nu \propto \nu^\alpha$. For two quasars, BR 0418−5723 and BR 2213−6729, no radio measurements are available.

[i] 1.4 GHz flux density from FIRST (Becker et al. 1995).

[j] 1.4 GHz flux density from NVSS (Condon et al. 1998).

[k] 1.4 GHz flux density from Carilli et al. (2001).

changed to $\alpha = -0.5$ (e.g., Schneider et al. 2001; Vanden Berk et al. 2001).

Column (6).—The absolute *B*-band magnitude computed using $\alpha = -0.79$. When $\alpha = -0.5$ is adopted for the extrapolation, the absolute *B*-band magnitudes are fainter by ≈0.35 mag.

Columns (7) and (8).—The observed count rate in the 0.5–2 keV band and the corresponding flux, corrected for Galactic absorption and the quantum efficiency decay of *Chandra* ACIS at low energy. The fluxes have been calculated using PIMMS (Mukai 2002) and a power-law model with $\Gamma = 2.0$; this is a good parameterization of samples of $z \approx 0$–3 quasars (e.g., George et al. 2000; Reeves & Turner 2000; Page et al. 2003; Piconcelli et al. 2005) and $z > 4$ quasars (V03b; V03c; see § 6).

Columns (9) and (10).—The rest-frame 2 keV flux density and luminosity, computed assuming $\Gamma = 2.0$ and corrected for the quantum efficiency decay of *Chandra* ACIS at low energy.

Column (11).—The 2–10 keV rest-frame luminosity.

Column (12).—The optical-to-X-ray power-law slope, α_{ox}, defined as

$$\alpha_{ox} = \frac{\log(f_{2\ keV}/f_{2500\ Å})}{\log(\nu_{2\ keV}/\nu_{2500\ Å})}, \quad (1)$$

where $f_{2\ keV}$ and $f_{2500\ Å}$ are the rest-frame flux densities at 2 keV and 2500 Å, respectively. The ≈1 σ errors on α_{ox} have been computed following the "numerical method" described in § 1.7.3 of Lyons (1991) considering both the statistical uncertainties on the X-ray count rates and the effects of reasonable changes in the X-ray and optical continuum shapes (see § 3 of V01a for details).

Column (13).—The radio-loudness parameter (e.g., Kellermann et al. 1989), defined as $R = f_{5\ GHz}/f_{4400\ Å}$ (rest frame). The rest-frame 5 GHz flux density was computed from the Faint Images of the Radio Sky at Twenty centimeters survey (FIRST; Becker et al. 1995), the NRAO VLA Sky Survey (NVSS; Condon et al. 1998) or the Carilli et al. (2001) observed 1.4 GHz flux density, assuming a radio power-law slope of $\alpha = -0.8$. The upper limits are at the 3 σ level. The rest-frame 4400 Å flux density was computed from the $AB_{1450(1+z)}$ magnitude, assuming an optical power-law slope of $\alpha = -0.79$. Typical radio-loudness values are >100 for radio-loud quasars (RLQs) and <10 for radio-quiet quasars (RQQs).

For the two quasars with the lowest declinations, BR 0418−5723 and BR 2213−6729, no sensitive radio data are available. None of the remaining quasars is radio-loud.

5. X-RAY PROPERTIES OF THE SAMPLE

In our previous study of a sample of optically luminous ($M_B \approx -28.4$ to -30.2) $z > 4$ PSS quasars (V03b), we derived the basic X-ray properties for some of the most luminous objects in the universe and performed joint X-ray spectral fitting. No spectral evolution in quasar X-ray continua at high redshift was found. With the current sample of 11 PSS and BRI quasars, our goal is to improve the results presented in V03b. The new *Chandra* observations, coupled with some other observations retrieved from the archive,[10] have increased the number of X-ray-detected AGNs at $z \gtrsim 4$ (mostly quasars) to ≈90. Overall, *Chandra* has detected ≈85% of the high-redshift quasars observed with snapshot observations. The program of snapshot

[10] See http://www.astro.psu.edu/users/niel/papers/highz-xray-detected.dat for a regularly updated compilation of X-ray detections and tight upper limits at $z \gtrsim 4$. Details about the analyzed *Chandra* archival observations are reported in Appendix B.

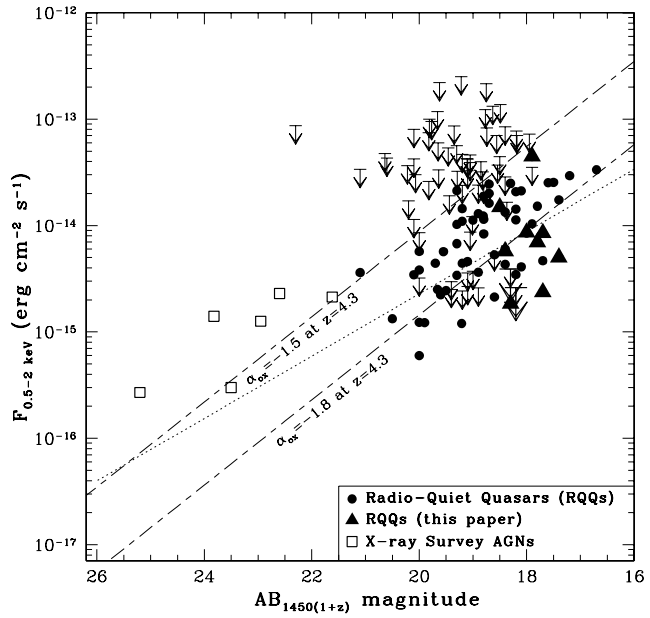

FIG. 3.—Observed-frame, Galactic absorption–corrected 0.5–2 keV flux versus $AB_{1450(1+z)}$ magnitude for $z \geq 3.96$ radio-quiet AGNs, mainly quasars. The objects presented in this paper are shown as triangles (X-ray detections) and large downward pointing arrows (upper limits); RQQs from previous X-ray observations (Kaspi et al. 2000; V01; Brandt et al. 2002; Bechtold et al. 2003; V03b; V03c) are shown as circles (X-ray detections) and small downward pointing arrows (upper limits). AGNs detected by X-ray surveys (Schneider et al. 1998; Silverman et al. 2002; V02; Castander et al. 2003; Treister et al. 2004) are shown as open squares. The slanted dashed lines show the $\alpha_{ox} = -1.5$ and -1.8 loci at $z = 4.3$ (the average redshift of the present sample); the dotted line shows the best-fit correlation reported in § 5 for the sample of high-redshift, optically selected RQQs observed by *Chandra*.

observations has allowed filling of the soft X-ray flux versus $AB_{1450(1+z)}$ plot shown in Figure 3 with many X-ray detections over the last few years. This plot is effective in showing the large advances made recently in the knowledge of the properties of high-redshift quasars (only RQQs are reported); for comparison, note the paucity of data points in Figure 2 of Brandt et al. (2001). Most of the upper limits shown in Figure 3 have been obtained using archival *ROSAT* observations; some of these are reported here for the first time (see Appendix A and Table 5 for details).

Most of the quasars presented in this paper (triangles in Fig. 3 for the nine X-ray detections and large downward pointing arrows for the two upper limits) populate the region close to the $\alpha_{ox} = -1.80$ slanted line (computed assuming $z = 4.3$, the average redshift of the current sample). They have an average $\langle \alpha_{ox} \rangle = -1.88 \pm 0.05$ (computed using the ASURV software package revision 1.2; LaValley et al. 1992; the quoted errors represent the standard deviation of the mean), which is steeper than the average value found using the whole population of RQQs at high redshift with available X-ray information ($\langle \alpha_{ox} \rangle = -1.76 \pm 0.02$).

This finding is consistent with the fact that the current *Chandra* sample is highly luminous ($\langle \log l_{2500} \rangle = 32.1$ ergs s^{-1} Hz^{-1}), and from previous work (e.g., Avni et al. 1995; Vignali et al. 2003a, hereafter VBS03; see also I. Strateva et al. 2005) α_{ox} has been found to depend on optical luminosity, i.e., more optically luminous quasars have steeper (more negative) α_{ox}. The expected α_{ox} for the current sample would be $\approx -1.8 \pm 0.1$. We note that α_{ox} for BR 0353−3820 is flat ($\alpha_{ox} = -1.54^{+0.07}_{-0.06}$), much below the average value for the whole sample; it is possible that this flat α_{ox} is due to some source variability occurring over the time interval between the optical and X-ray observations.

As discussed in previous works (e.g., V01a; V03c), there is a correlation between $AB_{1450(1+z)}$ and 0.5–2 keV flux (see Fig. 3). To have a homogeneous sample, we have used only the $z \gtrsim 4$ optically selected RQQs observed by *Chandra*; the significance of the correlation has been evaluated using the methods within ASURV, in particular, the generalized Kendall's τ (Brown et al. 1974). The $AB_{1450(1+z)}$ versus 0.5–2 keV flux correlation is significant at the >99.9% level; according to the estimate and maximize (EM; Dempster et al. 1977) regression algorithm, it can be parameterized by

$$\log (F_X/\text{ergs cm}^{-2}\ \text{s}^{-1}) = -(0.293 \pm 0.057)\text{AB}_{1450(1+z)} - (8.786 \pm 1.059),$$

plotted as a dotted line in Figure 3.

Figure 3 also highlights the large discrepancy in our knowledge of the properties of the high-redshift AGN population in its entirety. While X-ray information is presently available for large numbers of optically luminous quasars at $z \gtrsim 4$ (i.e., those located on the right-hand side of Fig. 3 and plotted as filled symbols and downward pointing arrows), only a few AGNs at fainter optical magnitudes are detected in the X-rays (*squares*). These have all been discovered by moderately deep and deep X-ray surveys with *ROSAT* (Schneider et al. 1998) and *Chandra* (Silverman et al. 2002; V02; Castander et al. 2003; Treister et al. 2004).

Two quasars in the present sample have not been detected by *Chandra*: PSS 1506+5220 (discussed in § 2.1) and PSS 2344+0342 (no X-ray counts within a 2″ radius circle). There are two possible explanations for the nondetections of these two quasars in the X-ray band: they are either strongly absorbed or intrinsically X-ray weak. If their nondetection is due to the presence of intrinsic X-ray absorption, then column densities of $N_H \gtrsim 1.5 \times 10^{23}$ and $\gtrsim 3.3 \times 10^{23}$ cm^{-2}, respectively, are required to reproduce the *Chandra* constraints (using the optical-to-X-ray correlation of VBS03 and assuming a photon index $\Gamma = 2.0$). It is interesting to note that the HET spectrum of PSS 1506+5220 displays a number of notable and complex features, the most prominent being broad, deep Si IV and C IV absorption lines. For the other X-ray-undetected quasar of the present sample, PSS 2344+0342, the optical spectrum shows two very high column density damped Lyα absorption (DLA) systems (Peroux et al. 2001; Prochaska et al. 2003); however, these are unlikely to be responsible for all of the absorption suggested by the X-ray constraints (see, e.g., Elvis et al. 1994 for discussion on the expected X-ray absorption by DLAs). We also note that the X-ray-weak BR 1117−1329 (detected with two counts; see § 2.1 and Table 2) shows blueshifted broad absorption lines for O VI, N V, Si IV, and C IV (Storrie-Lombardi et al. 1996).

6. JOINT SPECTRAL FITTING: A QUASAR X-RAY SPECTRAL TEMPLATE AT $z \approx 4$–6.3

Previous studies have provided basic information on the X-ray spectral properties of luminous, optically selected $z > 4$ RQQs, in particular, on their photon indices and column densities. These results have been achieved either with direct X-ray spectral fitting of a few X-ray-luminous quasar spectra observed with *XMM-Newton* (e.g., Ferrero & Brinkmann 2003; Grupe et al. 2004; Farrah et al. 2004) and *Chandra* (Schwartz & Virani 2004) or using joint X-ray spectral-fitting analysis, i.e., simultaneous fitting of sizable numbers of *Chandra* spectra of $z > 4$

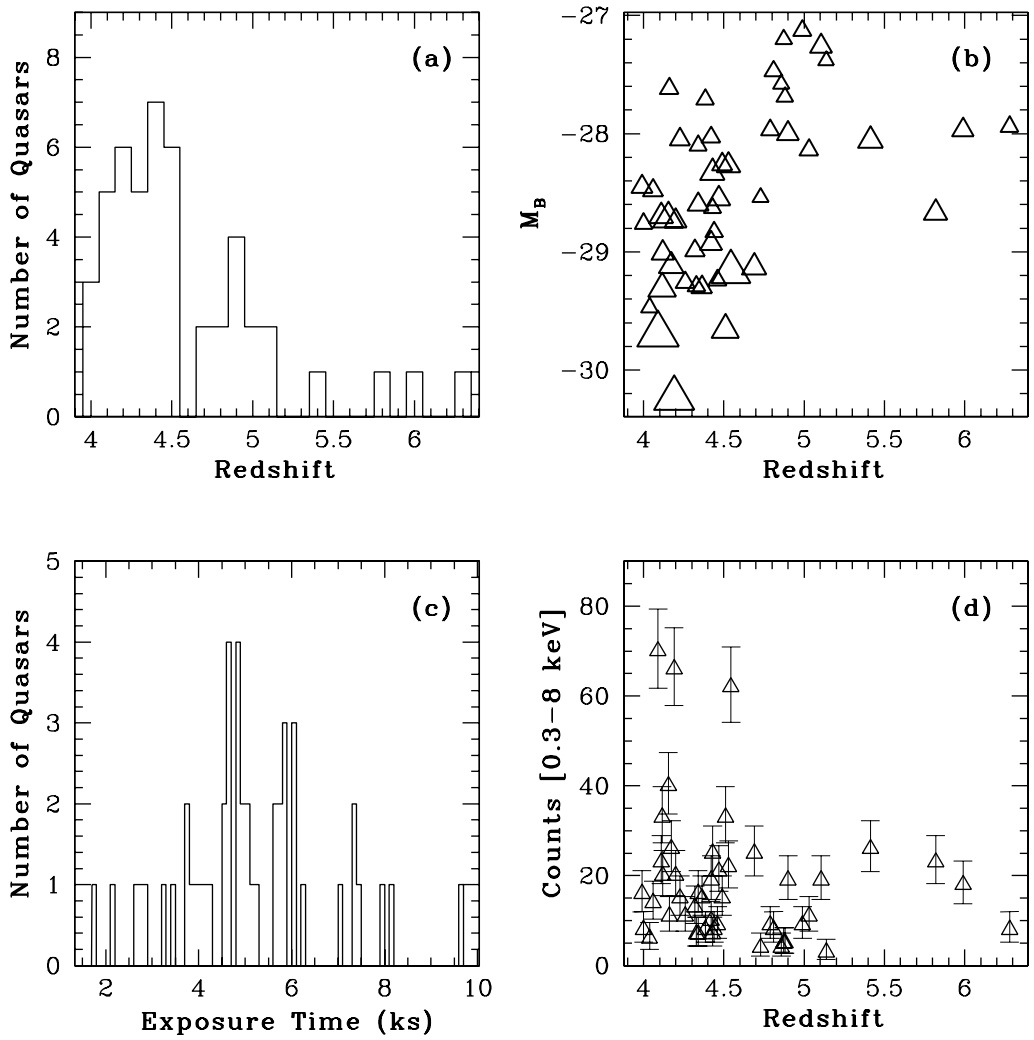

FIG. 4.—Relevant information for the 48 quasars used in the X-ray spectral analysis: (*a*) histogram of redshift; (*b*) redshift vs. absolute *B*-band magnitude (the sizes of the symbols increase with the number of counts); (*c*) histogram of the exposure times (corrected for detector dead time); (*d*) redshift vs. number of counts and relative errors (computed following Gehrels 1986).

quasars (e.g., V03b; V03c; Vignali et al. 2004). Since these objects are among the most luminous quasars at $z > 4$, they do not represent the majority of the high-redshift quasar population.

Like low- and intermediate-redshift RQQs (e.g., George et al. 2000; Reeves & Turner 2000; Page et al. 2003; Piconcelli et al. 2005), high-redshift RQQs are, on average, characterized by power-law continua with $\Gamma \approx 1.8-2.0$, with no indication of widespread absorption. Joint X-ray spectral-fitting studies are important, given the difficulty in obtaining quality X-ray spectra of high-redshift quasars using reasonable exposures (≈40–60 ks) with *XMM-Newton*. Furthermore, combining the spectra of many high-redshift quasars is a practical way to derive their average X-ray spectral properties; in fact, studies limited to a few X-ray-luminous quasars may not be representative of the high-redshift quasar population as a whole.

To provide further constraints on the average X-ray properties of high-redshift quasars, we have performed joint fitting using all the available *Chandra* data for RQQs in the redshift range $z = 3.99-6.28$. Neither X-ray-selected quasars (see V02 for X-ray spectral analyses of X-ray selected $z > 4$ AGNs in the Chandra Deep Field–North) nor radio-selected quasars (with the exception of FIRST 0747+2739, which is radio-quiet; see Bassett et al. 2004) have been considered in the following analysis. Source counts have been extracted for each quasar using a circular region of $2''$ radius centered on the X-ray centroid of the quasar. Although background is typically negligible in these *Chandra* observations, we have extracted background counts using annuli of different sizes (to avoid contamination from nearby X-ray sources) centered on the quasar position. Only sources with >2 full-band counts have been considered in the analysis. The selection criteria adopted in this study (mainly the RQQ selection and the fact that only *Chandra* data are used) reduced the number of $z \gtrsim 4$ quasars with usable X-ray information from ≈90 to 48, for a total exposure time of 244.1 ks. We have ≈870 net source counts in the observed 0.3–8 keV band, corresponding to the rest-frame ≈1.5–58 keV band; the average number of counts per object is ≈18.

Figure 4 summarizes the principal properties of the sample used in this X-ray spectral study. The average redshift of the sample is $z = 4.57$, while its median is $z = 4.43$.

Spectral analysis was carried out with XSPEC version 11.3.0 (Arnaud 1996) using unbinned data and the *C*-statistic (Cash 1979); this statistical approach allows one to retain all spectral information and associate with each quasar its own Galactic absorption column density and redshift (for the fitting with intrinsic absorption, see below). Errors are quoted at the 90% confidence level for one interesting parameter ($\Delta C = 2.71$; Avni 1976; Cash 1979), unless stated otherwise. Solar abundances

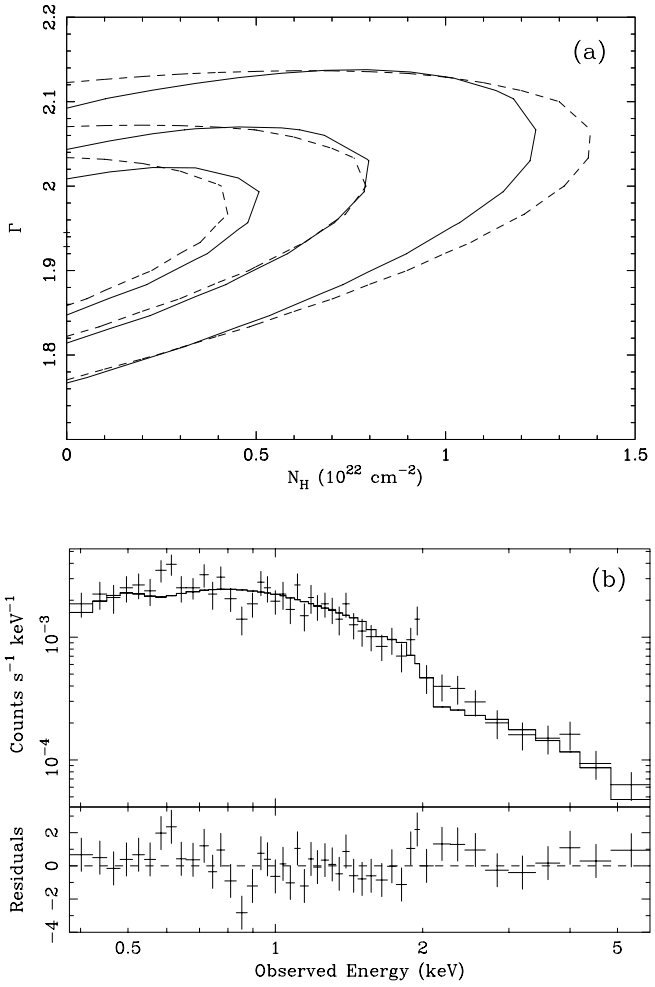

FIG. 5.—(*a*) 68%, 90%, and 99% confidence regions for the photon index vs. intrinsic column density derived from joint X-ray spectral fitting of the 48 RQQs at $z \geq 3.99$ detected by *Chandra* with more than 2 counts. The average redshift of the sample is $z = 4.57$, while its median redshift is $z = 4.43$. The solid contours have been obtained using all of the source counts, while the dashed contours show the results obtained in the rest-frame ≈2.2–40 keV band common to all of the quasars of the present sample. (*b*) Combined spectrum of the 48 RQQs at $z \geq 3.99$ fitted with a power law and Galactic absorption (*top*) and data-to-model residuals in units of σ (*bottom*).

(from Anders & Grevesse 1989) have been adopted for the absorbing material, although optical studies indicate that high-redshift quasars are often characterized by supersolar abundances of heavy elements (e.g., Hamann & Ferland 1999; Dietrich et al. 2003a, 2003b). Note that doubling the abundances in the fit produces a reduction in the column density of a factor of ≈2.

We started the joint X-ray spectral fitting using a power-law model, leaving the power-law normalizations for all of the quasars free to vary (to account for the different fluxes of the sources), plus Galactic absorption. The lack of significant data-to-model residuals for the fit suggests that the assumed model is acceptable; the resulting photon index, $\Gamma = 1.93 \pm 0.09$, is consistent with previous estimates for $z > 4$ quasars. The addition of neutral intrinsic absorption at each source's redshift does not improve the fit significantly; there is no evidence for widespread absorption toward the lines of sight of the quasars under investigation, the column density (i.e., the counts-weighted average column density) being $\lesssim 5.0 \times 10^{21}$ cm^{-2} (see the solid contours in Fig. 5*a* showing the 68%, 90%, and 99% confidence levels for the photon index vs. column density; see also Table 4). If our targets had intrinsic absorption of $N_{\rm H} \approx (2-5) \times 10^{22}$ cm^{-2}, as found in two RQQs at $z \approx 2$ using *ASCA* data (Reeves & Turner 2000), we would be able to detect it given the upper limit on the column density we derived. The spectral results do not change significantly if only the X-ray data in the rest-frame interval common to all of the quasars of the sample (≈2.2–40 keV band; ≈840 counts) are taken into account (see the dashed contours in Fig. 5*a*). In this case, the photon index is 1.95 ± 0.10, while the upper limit on the column density remains essentially unchanged.

The sample does not appear to be biased by the presence of a few high signal-to-noise ratio (S/N) objects.[11] This has been checked during the X-ray spectral analysis by removing some of the quasars with higher photon counting statistics. In particular, the removal of the three sources with ≳60 counts (BR 0353−3820, PSS 0926+3055, and PSS 1326+0743) leaves the photon index unchanged ($\Gamma = 1.92 \pm 0.10$), but the constraint on the column density intrinsic to the quasars is less tight ($\lesssim 7.5 \times 10^{21}$ cm^{-2}; see Table 4). We also performed joint spectral fitting using the most and least optically luminous RQQs of the sample, as well as the highest and lowest redshift RQQs; the results of the fitting are reported in Table 4. Within the statistical uncertainties from the limited number of X-ray counts, no evidence for a significant dependence of the X-ray spectral parameters on either the luminosity or the redshift of the quasar subsample has been found.

Given the limited counting statistics available and the fact that a power-law model seems to be acceptable, we did not investigate more complex spectral models. The typical upper limits on the EW of a narrow, either neutral or ionized, iron Kα line are not stringent, lying in the range ≈270–370 eV.

[11] For this reason, we have considered the ≈8.1 ks *Chandra* observation of SDSS 130608.26+035626.3 (Brandt et al. 2002) instead of the longer (≈120 ks) observation presented recently by Schwartz & Virani (2004).

TABLE 4
RESULTS FROM JOINT SPECTRAL FITTING

Quasars Used in the Fitting	Number of Quasars	Median z	Median M_B	X-Ray Counts	Γ	$N_{{\rm H},z}$[a] (cm^{-2})
All RQQs[b]	48	4.43	−28.54	872	$1.93^{+0.10}_{-0.09}$	$<4.95 \times 10^{21}$
All but the three highest S/N QSOs	45	4.43	−28.48	674	1.92 ± 0.10	$<7.48 \times 10^{21}$
Most optically luminous half of the sample	24	4.30	−29.06	563	$1.97^{+0.13}_{-0.10}$	$<6.50 \times 10^{21}$
Least optically luminous half of the sample	24	4.60	−28.25	309	$1.88^{+0.18}_{-0.15}$	$<1.19 \times 10^{22}$
Highest redshift half of the sample	24	4.83	−28.10	373	$1.98^{+0.19}_{-0.16}$	$<1.76 \times 10^{22}$
Lowest redshift half of the sample	24	4.20	−28.75	499	1.92 ± 0.12	$<4.86 \times 10^{21}$

[a] Column density in the quasar rest frame.
[b] The slightly different spectral-fit result reported in § 6 ($\Gamma = 1.93 \pm 0.09$) is referred to the power-law model without absorption.

Using the parameterization of the anticorrelation between the EW of the iron Kα line and source X-ray luminosity (the "X-ray Baldwin effect"; see Iwasawa & Taniguchi 1993 and Nandra et al. 1997) recently reported by Page et al. (2004), we would expect EW $\approx$ 50 eV for our sample of RQQs; their average rest-frame 2–10 keV luminosity is $10^{45.3}$ ergs s^{-1}. The expected EW is below the upper limits provided by joint X-ray spectral fitting.

To investigate the reliability of the joint X-ray spectral-fitting results, we performed two consistency checks. First, we compared the photon index obtained from the joint spectral fitting with that derived from band-ratio analysis (i.e., the ratio of the 2–8 to 0.5–2 keV counts, corrected for the ACIS quantum efficiency decay); for the Galactic column density, we assumed the average value for the 48 quasars weighted by the exposure time of each observation. The resulting photon index, $\Gamma = 1.89 \pm 0.08$ (the uncertainty quoted here corresponds to the 1 σ level; see Gehrels 1986 and footnote b of Table 2), is consistent with our previous value. Second, we added all of the source and background counts using the FTOOL task *mathpha*; similarly, redistribution matrix files and auxiliary response files were combined using *addrmf* and *addarf*, respectively, weighted by the individual exposure times. In this case the source counts were grouped into a spectrum such that each spectral bin contained at least 15 counts to allow χ^2 fitting. Our fitting obtained $\Gamma = 1.97 \pm 0.11$ and no evidence for intrinsic absorption ($N_{\rm H} \lesssim 4.4 \times 10^{21}$ cm^{-2}), as for the previously adopted fitting procedures. The power-law model and the data-to-model residuals are shown in Figure 5*b*.

Figure 6*a* shows the hard photon index (to avoid spectral complexities such as soft excesses at low energies) as a function of redshift for a compilation of optically selected RQQs. In particular, at low ($z < 1.8$) redshift we have used the X-ray spectral information for the Bright Quasar Survey (PG; Schmidt & Green 1983) objects presented by Piconcelli et al. (2005; *circles*); a few sources with Seyfert-like luminosity ($M_B > -23$) have been excluded from this analysis. At $z \approx 1.8-2.5$, the RQQs from the Vignali et al. (2001b) sample have been selected (*diamonds*). At the highest redshifts, the X-ray spectral results obtained over the last 3 yr with either joint spectral fitting (*triangles*) or individual observations (*squares*) are shown. The low-redshift ($z \lesssim 1$) quasars plotted in Figure 6*a* are usually $\approx$4 mag less luminous than the $z \gtrsim 4$ quasars under study; we are able to get down only to $z \approx 1$ with comparably luminous objects. Although significant intrinsic scatter in the photon indices at all redshifts is present, there is no detectable systematic change in the photon-index distribution at high redshift. The apparently smaller dispersion in the photon indices at high redshift than at lower redshift is at least partially due to the joint spectral fitting (used for some data points at $z > 4$), which tends to average any dispersion out. Although it is possible, in principle, that a redshift dependence of Γ could be canceled out by a luminosity dependence of Γ (which is not evident from Fig. 6*b*, where Γ is plotted against M_B), this would require somewhat of a conspiracy and cuts against Occam's razor. At present there is no overwhelming evidence that the photon index is significantly dependent on quasar X-ray luminosity; for further details, see the contrasting results presented by Dai et al. (2004) and Reeves & Turner (2000). A partial correlation analysis of the photon index versus redshift/X-ray luminosity for a large, uniformly selected sample of quasars is required to address this issue properly.

All of these spectral results confirm the lack of significant X-ray spectral evolution of luminous, optically selected quasars over cosmic time. Thus, despite the strong changes in environment and quasar number density that have occurred from $z \approx 0-6$, individual quasar X-ray emission regions seem to evolve relatively little (see Brandt et al. 2005).

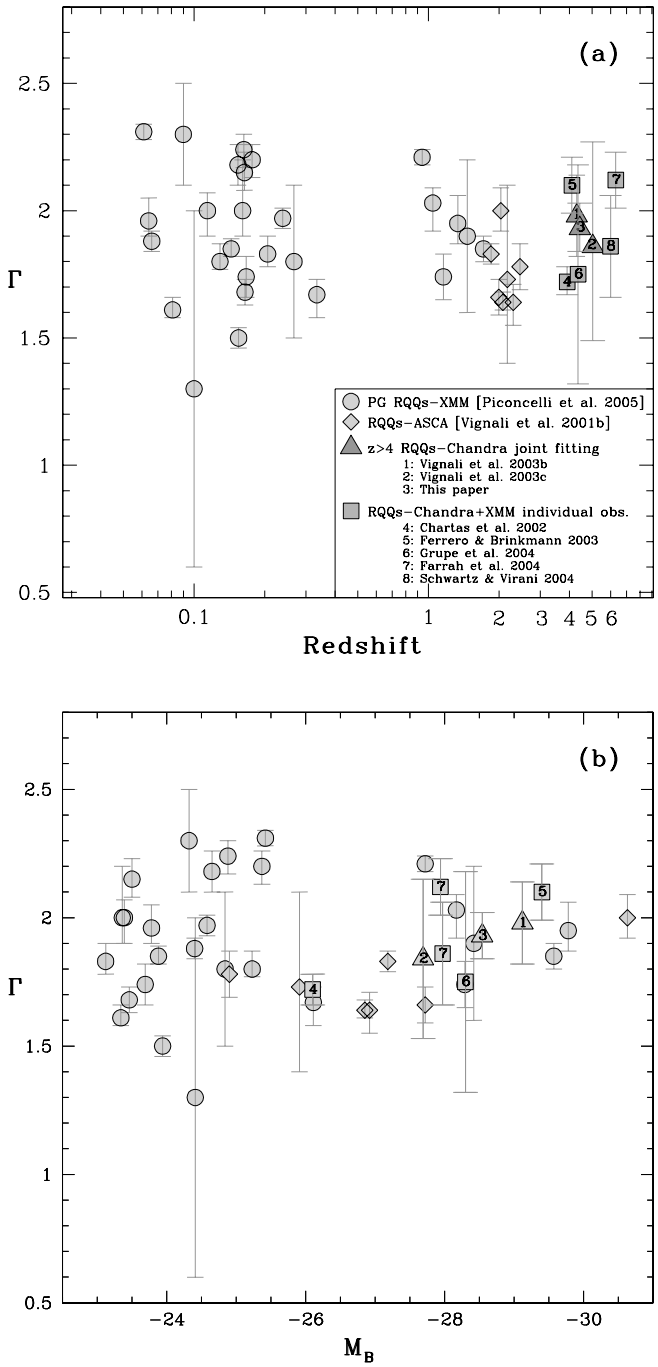

FIG. 6.—(*a*) Hard X-ray photon index vs. redshift for a compilation of RQQs. The circles at $z < 1.8$ indicate RQQs from the Bright Quasar Survey (PG) analyzed by Piconcelli et al. (2005), while the diamonds indicate the $z \approx 1.8-2.5$ RQQs from the Vignali et al. (2001b) sample. At higher redshift, the data points indicate joint spectral fitting (*triangles*) and single-object spectroscopy (*squares*); numbers in the data points correspond to the citations given in the figure legend. (*b*) Hard X-ray photon index vs. M_B for the same quasars.

7. X-RAY-UNDETECTED QUASARS: PECULIAR OBJECTS AT HIGH REDSHIFT?

Although the X-ray spectral results presented above are based on a significant fraction of the RQQs with *Chandra*

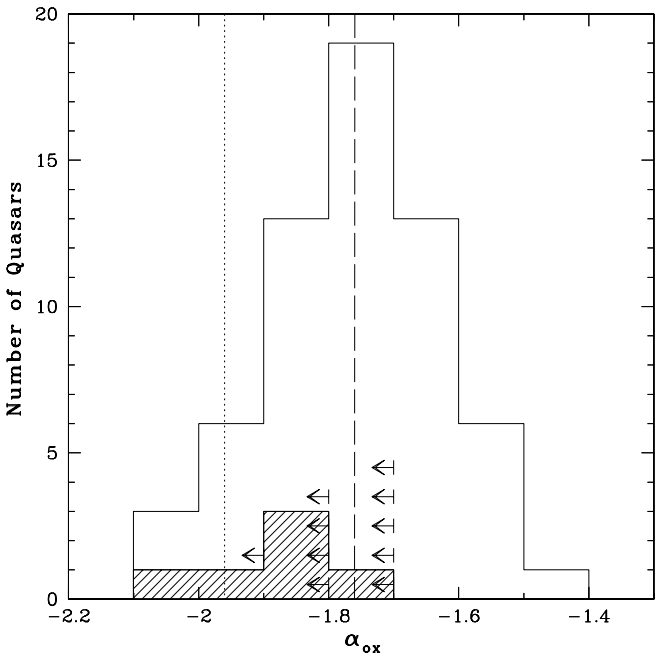

FIG. 7.—The α_{ox} distribution for the optically selected RQQs observed by *Chandra* at $z \geq 3.96$. Note that here we have also included the two-count source BR 1117−1329 at $z = 3.96$, which was not used in the joint X-ray spectral fitting. The hatched area indicates the BALQSOs; the areas with arrows indicate the 95% confidence upper limits. The long-dashed (*dotted*) line indicates the average α_{ox} (using ASURV) for high-redshift non-BAL RQQs (BALQSOs) observed by *Chandra*. The typical uncertainty in the α_{ox} measurements is ≈0.15.

observations, the selection of the sample might constitute a cause for concern, since we have excluded the faintest X-ray (with less than 2 counts) sources and nondetections. Overall, these X-ray-weak or undetected quasars represent ≈25% of the RQQ population thus far observed by *Chandra* at $z \gtrsim 4$. It is possible that in some cases the lack of an X-ray detection is due to absorption, which should be $\gtrsim 10^{23}$ cm^{-2} to reproduce the X-ray constraints (under reasonable assumptions about the spectrum). This is an acceptable explanation for BALQSOs (40% of the X-ray-undetected quasars; see Fig. 7). Past works have shown that BALQSOs are typically absorbed in the X-ray band (e.g., Brandt et al. 2000; Green et al. 2001; V01a; Gallagher et al. 2002).

In the α_{ox} histogram shown in Figure 7, BALQSOs preferentially populate the fainter part (i.e., more negative α_{ox} values) of the distribution. Although computed using a limited number of objects, their average α_{ox} (Fig. 7, *dotted line*) is -1.96 ± 0.06 (-1.92 ± 0.06 including SDSS 104433.04−012502.2 detected by *XMM-Newton*; see Brandt et al. 2001), while the optically selected non-BAL RQQs observed with *Chandra* have -1.76 ± 0.02 (Fig. 7, *long-dashed line*; the median value is −1.77). It is also plausible, although not necessarily required by the present data, that some of the remaining X-ray-undetected quasars at high redshift are characterized by absorption features that are not recognized because of either low spectral resolution (see, e.g., the case of SDSS 173744.87+582829.5 in V03c, where narrow absorption features were found with the HET) or limited spectral coverage (e.g., Maiolino et al. 2001, 2004; Goodrich et al. 2001). Given this, we believe that the criteria adopted in the selection of the high-redshift non-BAL RQQs for X-ray spectral analysis (see § 6) are not a cause for concern and that the results we derived can be considered representative of the RQQ population at $z \gtrsim 4$.

8. SUMMARY

We have analyzed *Chandra* observations of a sample of 11 quasars at $z \approx 3.96$–4.55 selected from the PSS and APM surveys. These are among the most luminous $z \gtrsim 4$ quasars known and represent ideal probes of the dawn of the modern universe. Given the optical luminosities of these quasars ($M_B \approx -28.5$ to -29.5), the present study can be considered complementary to past work (e.g., V03b; V03c). The principal results of this work are

1. Nine of the quasars have been detected, thus increasing the number of X-ray-detected AGNs at $z \gtrsim 4$ to ≈90. Including the two X-ray nondetections, the average α_{ox} of the present sample, -1.88 ± 0.05, is steeper than that typically found for $z \gtrsim 4$ quasars but consistent with the value expected applying the known dependence of this spectral index on quasar luminosity.

2. Two quasars, PSS 1506+5220 and PSS 2344+0342, are not detected. If absorption intrinsic to the source were the cause of the X-ray weakness of these two objects, then column densities larger than $N_H \approx 1.5 \times 10^{23}$ cm^{-2} would be implied. In the case of PSS 1506+5220, we found evidence for notable features, the most prominent being broad absorption lines from Si IV and C IV. For this source it is possible that the UV absorber is linked to the absorption likely present in the X-ray band. This has been observed before in other BALQSOs at high redshift.

3. Using all the available RQQs at $z \gtrsim 4$ detected by *Chandra* with more than 2 counts, we have derived X-ray spectral constraints for the quasar population at high redshift. A power law with $\Gamma = 1.93 \pm 0.09$ is a good parameterization of the quasar spectra in the rest-frame ≈2–40 keV band, similar to what is found for the hard X-ray continua of low- and intermediate-redshift quasars. Our results are consistent with a lack of significant spectral evolution of quasar X-ray continua over cosmic time. A partial correlation analysis of the photon index versus redshift/luminosity for a uniform sample of quasars over a broad range of redshift and luminosity is required to address this issue further.

4. The tight constraint on the absorption intrinsic to the quasars, $N_H \lesssim 5.0 \times 10^{21}$ cm^{-2}, indicates the lack of widespread obscuration.

The authors thank G. Djorgovski for kindly sharing data, G. Chartas and C. Peroux for useful discussions, L. Angeretti for help in producing the figures, and M. Mignoli for help with IRAF tasks. The authors thank the referee for his/her constructive comments.

C. V. acknowledges partial support from MIUR (COFIN grant 03-02-23). The financial support of NSF CAREER award AST 99-83783 (W. N. B.), CXC grant GO3-4143X (W. N. B.), and NSF grant AST 03-07582 (D. P. S.) is also acknowledged.

The HET is a joint project of the University of Texas at Austin, Pennsylvania State University, Stanford University, Ludwig-Maximillians-Universität München, and Georg-August-Universität Göttingen. The HET is named in honor of its principal benefactors, William P. Hobby and Robert E. Eberly. The Marcario Low-Resolution Spectrograph is named for Mike Marcario of High Lonesome Optics, who fabricated several optics for the instrument but died before its completion; it is a joint project of the HET partnership and the Instituto de Astronomía de la Universidad Nacional Autónoma de México.

APPENDIX A

NEW *ROSAT* UPPER LIMITS FOR $z > 4$ SDSS DR2 QUASARS

Here we report some additional X-ray flux upper limits for the Sloan Digital Sky Survey Data Release 2 (SDSS DR2; Abazajian et al. 2004) quasars at $z > 4$. These were obtained with *ROSAT* PSPC and HRI using only the inner $\approx 20'$ of these instruments. The 3 σ upper limits (see Table 5) have been derived in a similar way to those shown in Table 4 of V01a using the *sosta* command in the XIMAGE package (Giommi et al. 1992) version 4.2. The $AB_{1450(1+z)}$ magnitudes have been derived using the method described in § 2.2 of VBS03.

APPENDIX B

OPTICAL, X-RAY, AND RADIO PROPERTIES OF $z \geq 4$ QUASARS IN ARCHIVAL *CHANDRA* OBSERVATIONS

Here we report the main optical, X-ray, and radio properties for $z \geq 4$ quasars with unpublished *Chandra* observations (Table 6). Note that BR 1202−0725 was also detected by *ROSAT* (Kaspi et al. 2000).

TABLE 5
PROPERTIES OF $z > 4$ SDSS DR2 QUASARS IN *ROSAT* FIELDS

Object	z	$AB_{1450(1+z)}$	M_B	f_X[a]	α_{ox}	R[b]
SDSS 004054.65−091526.79	4.973	19.3	−27.6	<3.24	<−1.34	<5.6
SDSS 100645.60+462717.25	4.440	20.1	−26.7	<3.02	<−1.29	<136.7
SDSS 101053.00+531144.82	4.506	20.1	−26.7	<1.14	<−1.45	<10.1
SDSS 123735.47+642936.00	4.334	20.1	−26.6	<4.22	<−1.23	<32.7
SDSS 140146.53+024434.72	4.375	18.7	−28.0	<2.36	<−1.54	<2.8
SDSS 150730.63+553710.83	4.499	20.2	−26.6	<1.71	<−1.36	<11.1
SDSS 213243.26+010633.91	4.032	20.2	−26.4	<3.65	<−1.25	<10.5

[a] Galactic absorption–corrected flux in the observed 0.5–2 keV band in units of 10^{-14} ergs cm^{-2} s^{-1}.
[b] Radio-loudness parameter.

TABLE 6
OPTICAL, X-RAY, AND RADIO PROPERTIES OF $z \geq 4$ QUASARS IN ARCHIVAL *Chandra* OBSERVATIONS

Object	z	$AB_{1450(1+z)}$	f_{2500} Å	log $(L_{2500\ Å})$[a]	M_B	$f_{0.5-2\ keV}$	$f_{2\ keV}$	log $(L_{2\ keV})$[b]	log $(L_{2-10\ keV})$	α_{ox}	R
PSS 0134+3307	4.53	18.8	1.69	31.80	−28.3	11.5	9.45	27.55	45.44	−1.63	<8.1
PSS 0808+5215	4.44	18.2	2.93	32.03	−28.8	3.5	2.81	27.01	44.90	−1.93	0.2
BR 1202−0725	4.70	18.0	3.52	32.14	−29.1	8.5	7.21	27.45	45.34	−1.80	<1.3
BR 1600+0724	4.38	19.3	1.06	31.58	−27.7	6.8	5.43	27.28	45.21	−1.65	<3.4
BR 2235−0301[c]	4.25	18.9	1.54	31.72	−28.1	<2.6	<2.03	<26.84	<44.73	<−1.87	<8.5
PSS 2322+1944	4.12	17.9	3.86	32.09	−29.0	10.4	7.92	27.41	45.30	−1.80	0.2

NOTE.—Units are the same as in Table 3.
[a] Rest-frame 2500 Å luminosity density (ergs s^{-1} Hz^{-1}).
[b] Rest-frame 2 keV luminosity density (ergs s^{-1} Hz^{-1}).
[c] BALQSO.

REFERENCES

Abazajian, K., et al. 2004, AJ, 128, 502
Anders, E., & Grevesse, N. 1989, Geochim. Cosmochim. Acta, 53, 197
Arnaud, K. A. 1996, in ASP Conf. Ser. 101, Astronomical Data Analysis Software and Systems V, ed. G. Jacoby & J. Barnes (San Francisco: ASP), 17
Avni, Y. 1976, ApJ, 210, 642
Avni, Y., Worrall, D. M., & Morgan, W. A., Jr. 1995, ApJ, 454, 673
Bassett, L. C., Brandt, W. N., Schneider, D. P., Vignali, C., Chartas, G., & Garmire, G. P. 2004, AJ, 128, 523
Bauer, F. E., Alexander, D. M., Brandt, W. N., Schneider, D. P., Treister, E., Hornschemeier, A. E., & Garmire, G. P. 2004, AJ, 128, 2048
Bechtold, J., et al. 2003, ApJ, 588, 119
Becker, R. H., White, R. L., & Helfand, D. J. 1995, ApJ, 450, 559
Bertin, E., & Arnouts, S. 1996, A&AS, 117, 393
Brandt, W. N., Guainazzi, M., Kaspi, S., Fan, X., Schneider, D. P., Strauss, M. A., Clavel, J., & Gunn, J. E. 2001, AJ, 121, 591
Brandt, W. N., Laor, A., & Wills, B. J. 2000, ApJ, 528, 637
Brandt, W. N., Vignali, C., Lehmer, B. D., Lopez, L. A., Schneider, D. P., & Strateva, I. V. 2005, in Growing Black Holes, ed. A. Merloni, S. Nayakshin, & R. Sunyaev (Berlin: Springer), in press (astro-ph/0411355)
Brandt, W. N., et al. 2002, ApJ, 569, L5
Brown, B. W. M., Hollander, M., & Korwar, R. M. 1974, in Reliability and Biometry, ed. F. Proschan & R. J. Serfling (Philadelphia: SIAM), 327
Carilli, C. L., Bertoldi, F., Omont, A., Cox, P., McMahon, R. G., & Isaak, K. G. 2001, AJ, 122, 1679
Cash, W. 1979, ApJ, 228, 939
Castander, F. J., Treister, E., Maccarone, T. J., Coppi, P. S., Maza, J., Zepf, S. E., & Guzman, R. 2003, AJ, 125, 1689
Chartas, G., Brandt, W. N., Gallagher, S. C., & Garmire, G. P. 2002, ApJ, 579, 169
Cobos Duenas, F. J., Tejada, C., Hill, G. J., & Perez, G. F. 1998, Proc. SPIE, 3355, 424
Comerford, J. M., Haiman, Z., & Schaye, J. 2002, ApJ, 580, 63

Condon, J. J., Cotton, W. D., Greisen, E. W., Yin, Q. F., Perley, R. A., Taylor, G. B., & Broderick, J. J. 1998, AJ, 115, 1693
Dai, X., Chartas, G., Eracleous, M., & Garmire, G. P. 2004, ApJ, 605, 45
Dempster, A. P., Laird, N. M., & Rubin, D. B. 1977, J. Roy. Stat. Soc. B, 39, 1
Dickey, J. M., & Lockman, F. J. 1990, ARA&A, 28, 215
Dietrich, M., Appenzeller, I., Hamann, F., Heidt, J., Jäger, K., Vestergaard, M., & Wagner, S. J. 2003a, A&A, 398, 891
Dietrich, M., Hamann, F., Shields, J. C., Constantin, A., Heidt, J., Jäger, K., Vestergaard, M., & Wagner, S. J. 2003b, ApJ, 589, 722
Djorgovski, S. G., Gal, R. R., Odewahn, S. C., de Carvalho, R. R., Brunner, R., Longo, G., & Scaramella, R. 1998, in Wide Field Surveys in Cosmology, ed. S. Colombi & Y. Mellier (Paris: Editions Frontieres), 89
Eadie, W. T., Dryard, D., James, F. E., Roos, M., & Sadoulet, B. 1971, Statistical Methods in Experimental Physics (Amsterdam: North-Holland)
Ebeling, H., White, D. A., & Rangarajan, F. V. N. 2005, MNRAS, submitted
Elvis, M., Fiore, F., Wilkes, B., McDowell, J. C., & Bechtold, J. 1994, ApJ, 422, 60
Fan, X., et al. 2001, AJ, 121, 31
Farrah, D., Priddey, R., Wilman, R., Haenhelt, M., & McMahon, R. G. 2004, ApJ, 611, L13
Ferrero, E., & Brinkmann, W. 2003, A&A, 402, 465
Freeman, P. E., Kashyap, V., Rosner, R., & Lamb, D. Q. 2002, ApJS, 138, 185
Gallagher, S. C., Brandt, W. N., Chartas, G., & Garmire, G. P. 2002, ApJ, 567, 37
Garmire, G. P., Bautz, M. W., Ford, P. G., Nousek, J. A., & Ricker, G. R. 2003, Proc. SPIE, 4851, 28
Gehrels, N. 1986, ApJ, 303, 336
George, I. M., Turner, T. J., Yaqoob, T., Netzer, H., Laor, A., Mushotzky, R. F., Nandra, K., & Takahashi, T. 2000, ApJ, 531, 52
Giommi, P., Angelini, L., Jacobs, P., & Tagliaferri, G. 1992, in ASP Conf. Ser. 25, Astronomical Data Analysis Software and Systems I, ed. D. M. Worrall, C. Biemesderfer, & J. Barnes (San Francisco: ASP), 100
Goodrich, R. W., et al. 2001, ApJ, 561, L23
Green, P. J., Aldcroft, T. L., Mathur, S., Wilkes, B. J., & Elvis, M. 2001, ApJ, 558, 109
Grupe, D., Mathur, S., Wilkes, B., & Elvis, M. 2004, AJ, 127, 1
Hamann, F., & Ferland, G. 1999, ARA&A, 37, 487
Hill, G. J., Nicklas, H. E., MacQueen, P. J., Mitsch, W., Wellem, W., Altmann, W., Wesley, G. L., & Ray, F. B. 1998a, Proc. SPIE, 3355, 433
Hill, G. J., Nicklas, H. E., MacQueen, P. J., Tejada, C., Cobos Duenas, F. J., & Mitsch, W. 1998b, Proc. SPIE, 3355, 375
Irwin, M., McMahon, R. G., & Hazard, C. 1991, in ASP Conf. Ser. 21, The Space Distribution of Quasars, ed. D. Crampton (San Francisco: ASP), 117
Iwasawa, K., & Taniguchi, Y. 1993, ApJ, 413, L15
Kaspi, S., Brandt, W. N., & Schneider, D. P. 2000, AJ, 119, 2031
Kellermann, K. I., Sramek, R., Schmidt, M., Shaffer, D. B., & Green, R. F. 1989, AJ, 98, 1195
Kraft, R. P., Burrows, D. N., & Nousek, J. A. 1991, ApJ, 374, 344
LaValley, M., Isobe, T., & Feigelson, E. D. 1992, in ASP Conf. Ser. 25, Astronomical Data Analysis Software and Systems, ed. D. M. Worrall, C. Biemesderfer, & J. Barnes (San Francisco: ASP), 245
Lyons, L. 1991, Data Analysis for Physical Science Students (Cambridge: Cambridge Univ. Press)
Maiolino, R., Mannucci, F., Baffa, C., Gennari, S., & Oliva, E. 2001, A&A, 372, L5
Maiolino, R., Oliva, E., Ghinassi, F., Pedani, M., Mannucci, F., Mujica, R., & Juarez, Y. 2004, A&A, 420, 889
Mukai, K. 2002, PIMMS Users' Guide (Greenbelt: NASA/GSFC)
Nandra, K., George, I. M., Mushotzky, R. F., Turner, T. J., & Yaqoob, T. 1997, ApJ, 488, L91
Oke, J. B., & Gunn., J. E. 1983, ApJ, 266, 713
Omont, A., Cox, P., Bertoldi, F., McMahon, R. G., Carilli, C., & Isaak, K. G. 2001, A&A, 374, 371
Page, K. L., O'Brien, P. T., Reeves, J. N., & Turner, M. J. L. 2004, MNRAS, 347, 316
Page, K. L., Turner, M. J. L., Reeves, J. N., O'Brien, P. T., & Sembay, S. 2003, MNRAS, 338, 1004
Peroux, C., Storrie-Lombardi, L. J., McMahon, R. G., Irwin, M., & Hook, I. M. 2001, AJ, 121, 1799
Piconcelli, E., Jimenez-Bailon, E., Guainazzi, M., Schartel, N., Rodriguez-Pascual, P. M., & Santos-Lleó, M. 2005, A&A, 432, 15
Prochaska, J. X., Gawiser, E., Wolfe, A. M., Cooke, J., & Gelino, D. 2003, ApJS, 147, 227
Ramsey, L. W., et al. 1998, Proc. SPIE, 3352, 34
Rees, M. J. 1999, in After the Dark Ages: When Galaxies Were Young (the Universe at $2 < z < 5$), ed. S. Holt & E. Smith (New York: AIP), 13
Reeves, J. N., & Turner, M. J. L. 2000, MNRAS, 316, 234
Schlegel, D. J., Finkbeiner, D. P., & Davis, M. 1998, ApJ, 500, 525
Schmidt, M., & Green, R. F. 1983, ApJ, 269, 352
Schneider, D. P., Schmidt, M., Hasinger, G., Lehmann, I., Gunn, J. E., Giacconi, R., Trümper, J., & Zamorani, G. 1998, AJ, 115, 1230
Schneider, D. P., et al. 2001, AJ, 121, 1232
Schwartz, D. A., & Virani, S. N. 2004, ApJ, 615, L21
Silverman, J. D., et al. 2002, ApJ, 569, L1
Spergel, D. N., et al. 2003, ApJS, 148, 175
Strateva, I. V., Brandt, W. N., Schneider, D. P., Vanden Berk, D. G., & Vignali, C. 2005, AJ, submitted (astro-ph/0503009)
Storrie-Lombardi, L. J., Irwin, M. J., McMahon, R. G., & Hook, I. M. 2001, MNRAS, 322, 933
Storrie-Lombardi, L. J., McMahon, R. G., Irwin, M. J., & Hazard, C. 1996, ApJ, 468, 121
Treister, E., Castander, F. J., Maccarone, T. J., Herrera, D., Gaiser, E., Maza, J., & Coppi, P. S. 2004, ApJ, 603, 36
Vanden Berk, D. E., et al. 2001, AJ, 122, 549
Vignali, C., Bauer, F. E., Alexander, D. M., Brandt, W. N., Hornschemeier, A. E., Schneider, D. P., & Garmire, G. P. 2002, ApJ, 580, L105 (V02)
Vignali, C., Brandt, W. N., Fan, X., Gunn, J. E., Kaspi, S., Schneider, D. P., & Strauss, M. A. 2001a, AJ, 122, 2143 (V01a)
Vignali, C., Brandt, W. N., & Schneider, D. P. 2003a, AJ, 125, 433 (VBS03)
———. 2004, in ASP Conf. Ser. 311, AGN Physics with the Sloan Digital Sky Survey, ed. G. T. Richards & P. B. Hall (San Francisco: ASP), 317
Vignali, C., Brandt, W. N., Schneider, D. P., Garmire, G. P., & Kaspi, S. 2003b, AJ, 125, 418 (V03b)
Vignali, C., Comastri, A., Cappi, M., Palumbo, G. G. C., & Matsuoka, M. 2001b, in AIP Conf. Proc. 599, X-ray Astronomy: Stellar Endpoints, AGN, and the X-ray Background, ed. N. White, G. Malaguti, & G. Palumbo (New York: AIP), 999
Vignali, C., et al. 2003c, AJ, 125, 2876 (V03c)